Thermal Simulation for a Mechanical Spindle With External Cooler Across Grease Coated Interface

Liang Zhao
Xi'an Jiaotong University
Mohan Lei
Xi'an Jiaotong University
Hongdi Ren
Xi'an Jiaotong University
Jinshi Wang
Xi'an Jiaotong University
Shuai Wang
Xi'an Jiaotong University
Ben Q Li
Xi'an Jiaotong University
Jun Yang (softyj@163.com)
Xi'an Jiaotong Univeristy
Xuesong Mei
Xi'an Jiaotong University

Research Article

Keywords: Precision boring machine, Helical tube, Thermal error stabilization, Thermal equilibrium, Grease-coated interface

Posted Date: April 27th, 2021

DOI: https://doi.org/10.21203/rs.3.rs-437094/v1

Thermal simulation for a mechanical spindle with external cooler across grease coated interface

Liang Zhao[1, 2], Mohan Lei[3], Hongdi Ren[1, 2], Jinshi Wang[4], Shuai Wang[1, 2], Ben Q. Li[5], Jun Yang*[1, 2], Xuesong Mei[1, 2]

[1] State Key Laboratory for Manufacturing Systems Engineering, Xi'an Jiaotong University, Xi'an, 710049, China

[2] Shaanxi Key Laboratory of Intelligent Robots, Xi'an Jiaotong University, Xi'an, 710049, China

[3] School of Mechanical and Precision Instrument Engineering, Xi'an University of Technology, 710048, China

[4] State Key Laboratory of Multiphase Flow in Power Engineering, Xi'an Jiaotong University, Xi'an 710049, China

[5] Department of Mechanical Engineering, College of Engineering and Computer Science, University of Michigan, MI 48128, USA

Email: softyj@xjtu.edu.cn

Abstract

Spindles in precision boring machine often work in low speed and heavy load without internal cooling, and the thermal error is nonnegligible. So an external cooling system was designed, and the effectiveness of the designed scheme needs to be preliminarily verified by simulation before building the cooling system. Thermal simulations of the spindle with an external cooler require calculating the thermal resistance of the thermal grease-coated interface between the cooler and spindle. Models describing the contact thermal resistance and total thermal resistance for metal contact filled with silicone grease based on solid-liquid interface force equivalence were described in this paper, and experiments were also conducted to verify the accuracy of these models. The contact thermal resistances between the cast iron/copper and silicone grease on flat or arc surfaces were calculated, and the bulk thermal resistance of the silicone grease layer was calculated. The total heat transferred between the cooler and the silicone grease-coated interface of the spindle were calculated. Heat transfer and heat generation in the spindle were calculated, and a finite element model was established to verify the effectiveness of the designed external cooling scheme. Finally, results from experiments for the spindle in different conditions show that the external cooling system decreases the time to reach thermal equilibrium by more than 60%. The *RMSE* of the simulated thermal elongation is less than 5.7044 μm when the rotating speed of 3000 rpm, and is less than 3.9714 μm when the rotating speed is 1500 rpm.

Keywords Precision boring machine; Helical tube; Thermal error stabilization; Thermal equilibrium; Grease-coated interface

Nomenclature			
D	Outer diameter of the tube (mm)	P	External pressure (Pa)
d	Inner diameter of the tube (mm)	P_c	Capillary pressure (Pa)
L	Cooler length (m)	P_0	Atmospheric pressure (Pa)
S	Pitch (mm)	β	Notch slope angle (°)
s	Inter-tube spacing (mm)	φ	Grease-tube contact angle (°)
C	Diameter of the helical cooler	x	Penetration depth (μm)
R_c	Contact thermal resistance $(m^2 \cdot ℃/W)$	S_i	The *i*th peak-peak interval (μm)
A_{nominal}	Nominal contact area (m^2)	BLT	Grease layer thickness (mm)
A_{real}	Real contact area (m^2)	R_{bulk}	Bulk thermal resistance $(m^2 \cdot ℃/W)$
P_{anr}	Ratio of nominal-real contact area	R_{sm}	Mean peak-peak interval
k_1	Substrate thermal conductivity (W/m· ℃)	R_{tot}	Total thermal resistance $(m^2 \cdot ℃/W)$
k_2	Grease thermal conductivity (W/m· ℃)	C_{tot}	Total thermal conductance $(W/m^2 \cdot ℃)$
σ	Root mean square roughness (μm)	τ	Shear stress (N m^{-2})
γ	Surface tension	τ_0	Yield shear stress (N m^{-2})
		H	Thickness of the grease (mm)

1 Introduction

The most important factor that reduces the machining accuracy of precision machine tools is thermal error caused by an uneven temperature field distribution [1, 2]. At present, there are two methods for reducing the influence of thermal error in a spindle during operation. In the error compensation method, a model describing the thermal error of the spindle is determined using regression, numerical analysis, or empirically from experimental data, and the feed axis is adjusted using a computerized numerical control (CNC) system to implement compensation [1, 3]. In the temperature control method, circulating coolant is used to remove excessive heat from the spindle such that the temperature of the spindle is kept uniformly distributed, thereby reducing thermal error [1].

Comparing these two methods, thermal error compensation is more economical and convenient. It can be used to increase machining accuracy, and to decrease design and manufacturing costs. However, there are limitations in the scope and effectiveness of the compensation method, and the robustness to complex working conditions is poor [1]. In addition, thermal error compensation relies on specific CNC systems and compensators, and the compensation process is discrete and non-uniform [4].

The temperature control method uses circulating coolant which carries heat away

from the spindle and is known to be an effective method for suppressing thermal error [5]. In order to prevent an uneven temperature distribution in the structure of an electric spindle, we should tailor specific solutions to regulate the heat exchange between heat generating components, the processing environment, and spindle structure. One approach is to controlling the coolant flow inside the spindle [1,6]. These technologies have been shown to reduce thermal deformation by up to 40% and thermal error during machine tool operation from 5 to 3 μm. However, the company did not report relevant technical details, nor did it publish corresponding papers. Xia et al. used fractal theory to design a new type of fractal tree-like channel network heat sink, and they developed a three-dimensional thermal and hydrodynamic model for the heat sink. Compared with experimental results from a traditional helical channel heat sink, the fractal tree-like channel heat sink provides lower pressure drop, more uniform temperature field distribution, and higher coefficient of performance [7]. Liu et al. proposed a differentiated multi-loop bath recirculation cooling system. This cooling system includes customized coolant flow channels that are located near the heat source and heat-sensitive parts, such as the stator and bearing inside the main shaft. The system then adjusts the temperature of the coolant in each flow channel, through independent oil temperature controllers. Each temperature controller has a PID controller whose parameters of heating power are set based on the oil temperature difference between the outlet and inlet, and the cooling power is constant [8].

In summary, circulating coolant can be used to remove heat from high temperature areas in the spindle, which helps make the overall temperature distribution uniform, thereby suppressing thermal errors. This paper takes the mechanical spindle of a certain type of precision CNC boring machine as the research object. This machine tool is primarily used for drilling, tapping, and boring, particularly large-scale boring for bearing seat keyholes in transmission boxes. This spindle must operate at low speed and heavy load. Thereby a mechanical spindle without a built-in motor is selected. The rear servo motor also keeps the heat source away from the center of the spindle, but the heating of the bearing inside the spindle cannot be ignored. Results from experiments show that thermal error is up to 50 μm when the rotating speed is 3000 rpm without cooling, so the influence from thermal deformation is nonnegligible.

Therefore, an external cooling scheme using a helical tube cooler is presented in this paper. Parts of the spindle at high temperature, such as the outer ring of the bearing and motor stator, are usually in contact with the spindle sleeve and the spindle housing. Therefore, the helical tube cooler can dissipate a lot of heat from the spindle when the cooler is wound on the outside of the spindle housing, which reduces the temperature

of heat-sensitive parts like bearings. This also isolates heat from the shaft, so as to make the temperature distribution of the spindle uniform and stabilize the thermal error [9]. Meanwhile, in order to improve the heat transfer efficiency, the region between the cooler and the spindle housing was filled with a thermally conductive silicone grease. The helical coil tube cooler we designed is shown in Figure 1.

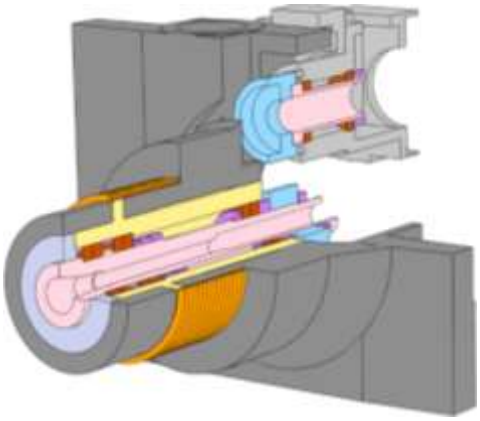

Figure 1. Helically coiled tube cooler.

To initially verify and optimize the external cooling scheme, we need to simulate the thermal characteristics of the spindle under cooling. The thermal resistance of the thermal grease-coated interface needs to be accurately calculated. The total thermal resistance of the coated joints is composed of the bulk thermal resistance of the silicone grease and the contact thermal resistance between the silicone grease and the substrate [10]. On the basis of quantities of experimental studies, Bajracharya et al. indicated that although the contact thermal resistance between the solid and silicone grease materials is usually smaller than the bulk thermal resistance of the silicone grease, the contact thermal resistance will still produce a non-negligible contact thermal resistance when the contact substrate surface, such as the outer surface of the spindle and other non-matching surfaces is rough [11].

Prasher et al. considered the wettability of grease on solid metal surfaces, analyzed the external, capillary, and air pressure equilibrium on the fluid-solid-air interface in detail, and simplified the surface roughness profile by defining a distribution of conical notches. These ideas were used to derive an analytical model describing the thermal resistance of a fluid-solid interface. Thermal resistance experiments were conducted with various thermal interface materials and substrates, and the model was found to produce results that were consistent with experimental results [12]. Hamasaiid et al. and Yuan Chao et al. proposed a fluid-solid interface contact thermal resistance model under the assumption that the surface roughness distribution is Gaussian [13-15]. Flat contact pairs coated with grease were considered in the aforementioned studies, but studies concerning the thermal resistance of coated cambered-flat contacts are not

present in the literature. Flat contact pairs coated with grease were considered in the aforementioned studies, but studies concerning the thermal resistance of coated cambered-flat contacts are not present in the literature. On the basis of the aforementioned research and previous work by our group [17, 18], considering the heat transfer rate of the grease coated helical tube-spindle housing interface, the finite element method was used for thermal-fluid-solid simulations of an externally cooled the spindle. Our simulation was used to determine the influence of different coolant temperatures on the temperature field and thermal error of the spindle. The thermal conductivity of a contact surface filled with silicone grease between the helical tube and the spindle housing is described in Section 2; the cooling system design is discussed in Section 3; simulations are described in Section 4; experimental results showing the effectiveness of the proposed temperature control method are presented in Section 5; conclusions are presented in Section 6.

2. Thermal resistance of the silicone grease interface between the external cooler and the spindle

2.1 Thermal resistance of solid metal coated with thermal grease

Due to microscopic and macroscopic irregularity in the surface morphology of metals, the real contact area between the solid metal joints usually accounts for only 1-2% of the nominal contact area. Gaps in the joints are filled with air, which has lower thermal conductivity than metal [10], thus the thermal resistance at the surface of a metal joint is usually large (Figure 2. (a)). Filling thermal interface materials between the metal joint surfaces, such as various types of thermally conductive silicone grease, can effectively reduce the thermal resistance between the metal joint surfaces (Figure 2. (b)).

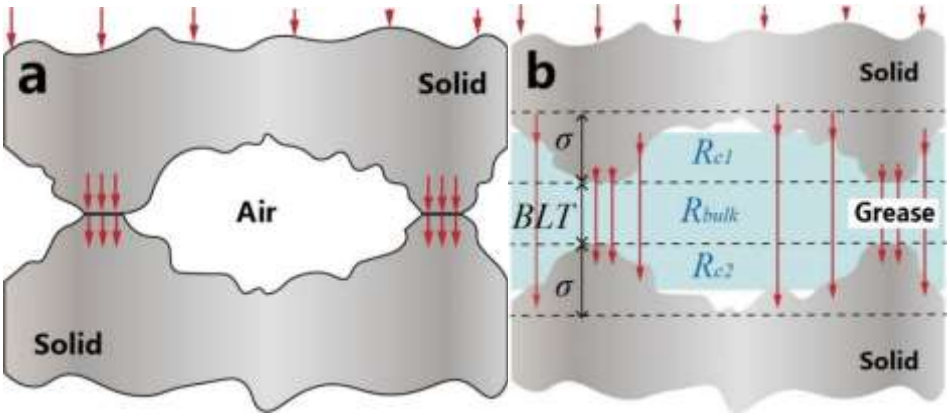

Figure 2. Heat conduction of joint surface; (a) rough metal joint surface and (b) metal

interface filled with silicone grease.

There is a linear positive correlation between the thermal resistance of the silicone grease and the thermal conductivity K of the silicone grease, and a negative linear correlation between the thermal resistance and the thickness of the silicone grease BLT (bond line thickness). The bulk thermal resistance in silicone grease is defined as follows [13, 19]:

$$R_{bulk} = \frac{BLT}{k} \tag{1}$$

The total thermal resistance R_{tot} of the joint surface per unit area can be considered a linear superposition of the thermal resistance R_{bulk} of the bulk silicone grease and the thermal contact resistance between the silicone grease and upper (R_{c1}) and lower (R_{c2}) substrates:

$$R_{tot} = R_{bulk} + R_{c1} + R_{c2} \tag{2}$$

Therefore, the total thermal conductance C_{tot} of the joint surface per unit area is:

$$C_{tot} = \frac{1}{R_{tot}} \tag{3}$$

In the simulation of the external spindle cooling system in this paper, in order to accurately show the effect of the external cooler on the thermal characteristics of the spindle under different cooling parameters, the total thermal resistance R_{tot} between the joint surfaces must be accurately calculated.

2.2 Contact thermal resistance between silicone grease and a metal substrate

The surface morphology of the helical tube cooler and spindle housing, as well as the physical properties of the selected thermal grease, will affect the effect of the cooler under certain circumstances. When the contact surface is rough and the contact pressure is low, the grease-substrate thermal resistance R_c may account for a large proportion of the total thermal resistance at the joint surface. Estimated R_c is vital for the simulation of spindle thermal behaviour under external cooling. Refer to Prasher's surface chemistry model [12]. The thermal resistance of a grease-substrate interface can be defined as follows:

$$R_c = \frac{k_1+k_2}{2k_1k_2}\left(\frac{A_{nominal}}{A_{real}}\right)\sigma \tag{4}$$

where k_1 is the thermal conductivity of the solid metal substrate, k_2 is the thermal conductivity of the silicone thermal grease, σ is the root mean square roughness of the rough substrate surface, $A_{nominal}$ is the nominal contact area, and A_{real} is the actual

microscopic contact area.

The nominal area and actual contact area are defined as follows:

$$A_{real} = \pi\sqrt{x^2 + (xcot\varphi)^2}(2r_0 - xcot\varphi) \tag{5}$$

$$A_{nominal} = \pi r_0\sqrt{r_0^2 + \sigma^2} \tag{6}$$

In Eqs. (5) and (6), x is the penetration depth of the liquid; σ is the root mean square of the surface roughness, which can also represent the depth of a conical notch; φ is defined in Figure 3.

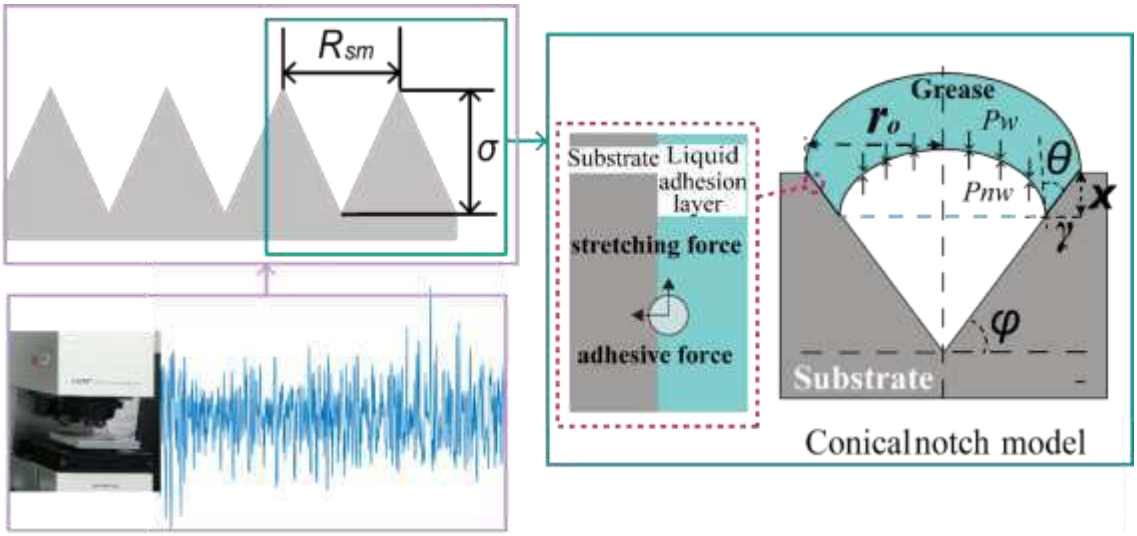

Figure 3. Conical groove model based on surface roughness.

When the adhesion force is greater than the cohesive force, the resultant force *F* on liquid molecules in the adhesion layer is perpendicular to the solid-liquid interface and points towards the solid, makes the liquid molecules in the adhesion layer receive more force than the molecules inside the liquid. Therefore, molecules in the adhesion layer should have a smaller potential energy than in the liquid. Because the potential energy will be minimum in a stable mechanical equilibrium, the molecules in the liquid should squeeze into the adhesion layer as much as possible and thus expand the adhesion layer. γ represents the surface tension in the contact interface, and γ acts on the gas-liquid interface along the solid-liquid-gas junction (circumference) (Figure 3). γ_{AL}, γ_{AS}, and γ_{LS} are the surface tensions at the gas-liquid, gas-solid, and liquid-solid interfaces, respectively. When the surface tensions are balanced, we have:

$$\gamma_{AS} = \gamma_{LS} + \gamma_{AL}cos\theta \tag{7}$$

among them, L represents the fluid (silicone grease), S represents the solid metal substrate, and A represents air. In Figure 3, P_{nw} is the pressure exerted by the non-

wetting phase, and P_{nw} is the pressure exerted by the wetting phase.

The rough surface can be simplified into a plane containing a large number of tiny conical notches (Figure 3). The capillary pressure generated by the fluid tension will push the silicone grease into the conical notches. The capillary pressure is defined as follows [12]:

$$P_c = \frac{2\gamma_{AL}\sin(\theta+\varphi)}{r_0 - x\cot\varphi} \tag{8}$$

Air trapped in the silicone grease in the conical notches cannot leave the conical notches, i.e., the conical notch is not open to the atmosphere, and the ideal gas law is still applicable to gas trapped in a conical notch. The volume of a spherical dome of air in a conical notch (Figure 3) is negligible compared to the volume of the conical notch. Then, a pressure equilibrium can form at the liquid-air interface, in which the external pressure P and the capillary pressure P_c toward the bottom of the conical notch will balance the back pressure exerted by air trapped in the notch. This equilibrium can be expressed by the following equation:

$$P + P_c = P_0 \frac{r_0^3}{(r_0 - x\cot\varphi)^3} \tag{9}$$

$$P + \frac{2\gamma_{AL}\sin(\theta+\varphi)}{r_0 - x\cot\varphi} = P_0 \frac{r_0^3}{(r_0 - x\cot\varphi)^3} \tag{10}$$

where P is the externally applied pressure, P_0 is the atmospheric pressure, x is the penetration depth into the liquid, and σ is the root mean square roughness of the rough surface and can represent the depth of a conical notch. One can eliminate the penetration depth x from Eqs. (9) and (10) to determine φ:

$$\varphi = arctan\frac{\sigma}{r_0} \tag{11}$$

In this paper, a confocal microscope was used to measure the rough surface morphology and determine σ and r_0. Each objective lens in a confocal microscope has its own unique surface roughness measurement range, which is determined by the working distance, depth of field, and pixel size. Some experimental results in the literature [20] provide guidance on selecting the magnification in the use of the confocal microscope for a given surface roughness R_a.

The ratio of nominal area to the actual area $p_{anr} = \frac{A_{nominal}}{A_{real}}$ can be calculated using measured values of x, φ, r_0, and σ. R_c can be finally obtained from $k_1$and $k_2$using Eq. (4).

When using a confocal microscope to observe the rough surface morphology of a flat sample, the measured morphology consists of roughness and waviness components. Because the profile signal measured from the rough metal surface contains roughness and waviness information, using the root mean square to characterize the rough profile will produce different results when different magnification values are used for observation.

We used $r_0 = \frac{R_{sm}}{2}$, where R_{sm} is the average spacing between profile peaks with respect to an average line measured within the sampling length. In other words, $R_{sm} = \frac{1}{N}\sum_{i=1}^{N} S_i$, where S_i is the distance between the i-th rough peak and the i+1th rough peak, as shown in Figure 4.

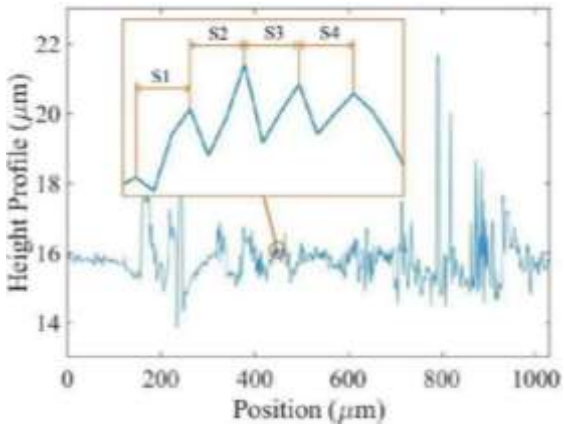

Figure 4. Average peak spacing in rough surface profile.

2.3 Verification of the contact thermal resistance model

The rough morphology of an aluminum-6061-T4 block substrate was examined with a confocal laser microscope (Olympus LEXT OLS4000) (Figure 5). According to experimental conclusions given in the literature [20], the roughness of the surface is large enough that a 10X magnification lens could be used for observation.

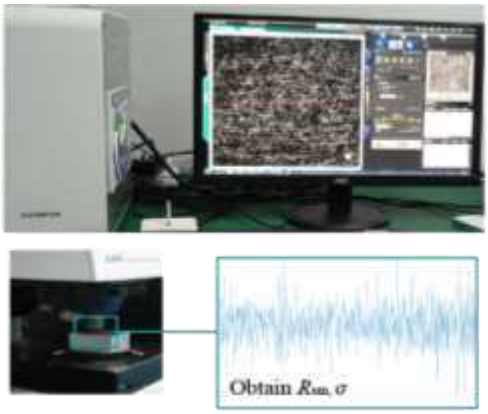

Figure 5. Rough topography measurement.

In the literature [21], a silicone grease-metal substrate contact thermal resistance experiment was conducted for aluminum-6061-T4 with 1.13 μm surface roughness. In this paper, the rough morphology of a similar aluminum-6061-T4 sample was measured. The measured root mean square roughness is $\sigma = 1.739$ μm, and the average peak spacing $R_{sm} = 10.119$ μm. Silicone grease (Dow Corning DOWSIL TC-5121) with thermal conductivity $k = 2.15 \frac{W}{m \cdot ℃}$ was used for verification. A comparison of the results shows that the calculated thermal resistance is consistent with the experimental results.

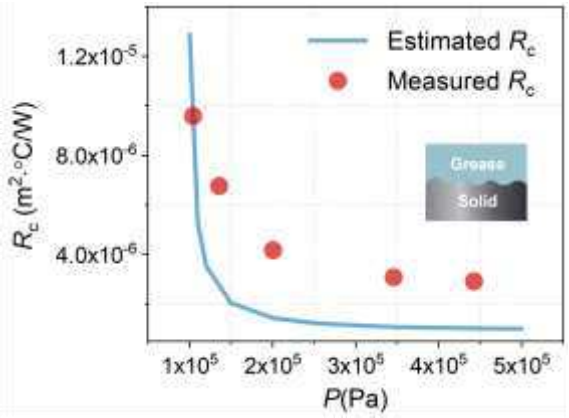

Figure 6. Comparison between calculated and experimental contact thermal resistance between aluminum and silicone grease.

2.4 Experimental verification of the interfacial thermal resistance model

The structure of the thermal conductivity tester used in verification experiments is shown in Figure 1. The system consists of four parts: heat flux meters, heating and cooling units, insulation material, and pressure components. The heat flux meters are used to measure the heat flow q passing through the specimen and the temperature

difference of the test interface. The area of the interface is 707 mm^2, and the thermal conductivity of the substrate is 380 $\frac{W}{m\cdot℃}$. Thermocouples were placed every 50 mm on the centerline of each flux meter, and the minimum distance between the thermocouple and the end face was set to 15 mm. Heat can flow along one dimension when the heating and cooling units are in operation. The insulation material was placed around the heat flux meters to prevent heat dissipation. A screw was used for pressurization and a pressure sensor was used for continuously monitoring the load. The thermal conductivity tester parameters are shown in Table 1.

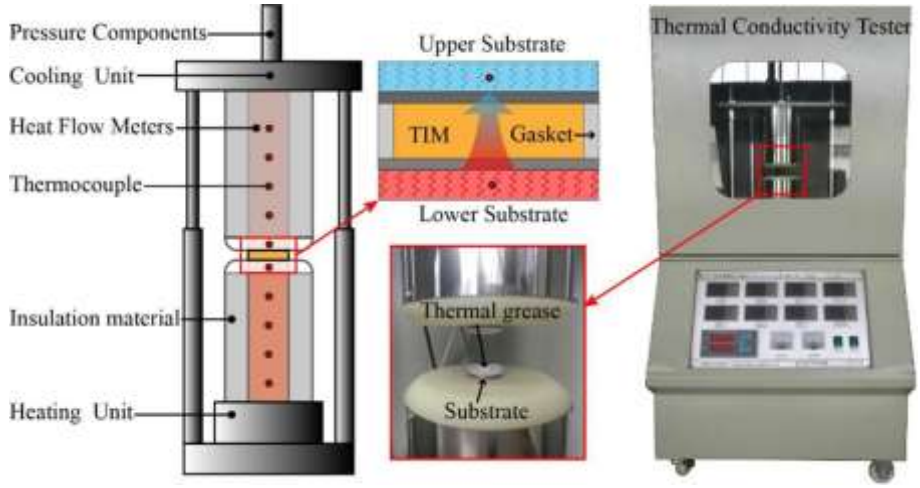

Figure 7. Silicone grease thermal conductivity tester

Table 1 Parameters of thermal conductivity tester

Distance between thermocouples	50	mm
Distance between the thermocouple and end face	15	mm
Thermal conductivity of heat flux meters	380	$\frac{W}{m\cdot℃}$
Cross sectional area of heat flux meters	707	mm^2
Instrument Correction Coefficient	1.0300	

The silicone grease was coated on the test interface, and insulating nylon gaskets with different thickness were used to support the upper and lower substrates. The thickness of the silicone grease was approximated as the thickness of the gasket. Important experimental parameters are shown in Table 2.

Table 2 Setting of experimental parameters and the test result

Average temperature T (℃)	Hot surface temperature TH (℃)	Cold surface temperature TC (℃)
51.36	62.52	40.20

The thermal resistance between the bonding surfaces of the copper substrate coated with thermal grease was measured. The thermal conductivity of the two test silicone greases are respectively k_1 = 0.79 $\frac{W}{m\cdot℃}$ and k_2 = 0.58 $\frac{W}{m\cdot℃}$. 4 gaskets with different thickness were used to adjust the thickness of the silicone grease during the experiment, and the thermal resistance of the joint surface was also measured. The thickness of each gasket was measured with a micrometer to be *BLT*1 = 0.115 mm, *BLT*2 = 0.155 mm, *BLT*3 = 0.214 mm, *BLT*4 = 0.301 mm. After analyzing the experiment results, we can conclude that the model is consistent with experimental thermal resistance measurements.

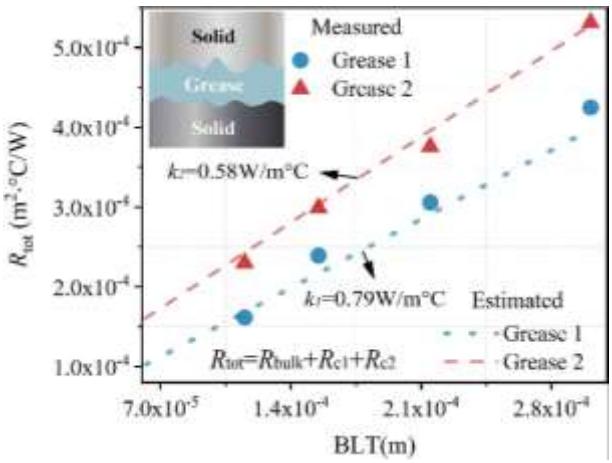

Figure 8. Comparison between calculated and experimental total thermal resistance between copper substrates filled with silicone grease.

3. Thermal simulation of helical tube-silicon grease-spindle system

3.1 TIM Thermal interface material（TIM）total thermal resistance

The thickness of the silicone grease between the external helical tube cooler and the spindle was measured to be b = 2.5 mm. The cross-section of the copper helical tube is approximately circular with 6 mm outer diameter, and the externally applied total normal force F exerted by a clamp on the helical tube was approximately 1000 N. The maximum contact angle in the cross-section of the helical tube-grease-spindle housing interface is φ_m, as shown in Figure 9.

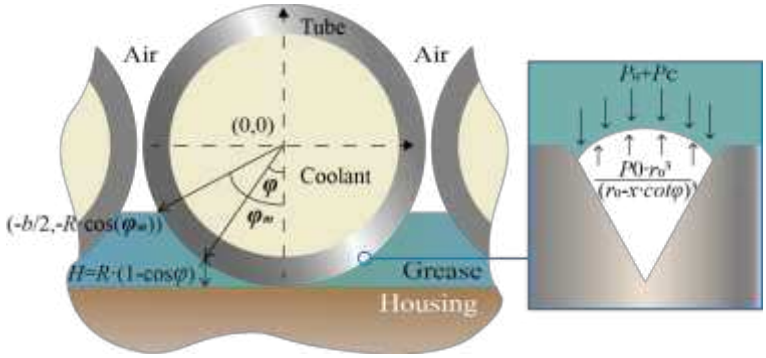

Figure 9. Copper tube-silicone grease-spindle shell contact cross section.

The thickness of the silicone grease layer between the copper tube and spindle housing was $H = h_t + h_{min}$, where h_{min} is the minimum thickness of the silicone grease layer and $h_t = R(1 - \cos\varphi)$, where φ is the contact angle, R is the outer diameter of the tube.

The thermally conductive grease exhibits Herschel-Bulkley fluid properties when x = 0, $\varphi = 0$, $h_t = 0$, $H = h_{min}$, as shown in Figure 9 [23]. The helical tube and spindle housing all remained stationary during the experiment, thus the silicone grease in the joint surface was kept stationary. The shear rate was γ_s = 0, and the shear stress τ is equivalent to the yield stress τ_0, i.e., $\tau = \tau_0 \approx 32.29\ N \cdot m^{-2}$. When the mass of the silicone grease is ignored, the *y* component of the grease shear stress is $P(\varphi) = \tau_0 \cdot sin\varphi$, and

$$F > L_t \cdot \int_{-\varphi_m}^{\varphi_m} P(\varphi) d\varphi \tag{12}$$

Grease flows until the helical tube is in solid contact with the housing, and the solid contact would bear the majority of the pressure from the clamp. One can infer that the minimum thickness of the grease layer in the coated joint surface is very small, i.e., $h_{min} \approx 0$. The bulk thermal conductivity of the silicone grease is $k_{bulk} = 0.5981(\frac{W}{m \cdot ℃})$, while the thickness of the silicone grease is:

$$H = h_t = R \cdot (1 - \cos\varphi) \tag{13}$$

The thermal resistance per unit area (m^2) of silicone grease in coated joints between the copper helical tube and the spindle housing is defined as follows :

$$R_{bulk} = \frac{R \cdot sin(\varphi_m) - R \cdot sin(-\varphi_m)}{\int_l^u \frac{k_{bulk}}{H}\, d\varphi} \tag{14}$$

where $\varphi_m = arccos\frac{R-b}{R}$.

Figure 9 shows the ratio of the contact area (surface area) between the silicone grease and the copper helical tube to the contact area (planar area) between the silicone grease and the spindle housing is p_{ca}:

$$p_{ca} = \frac{2 \cdot R \cdot sin\ \varphi_m}{2 \cdot \pi \cdot R \cdot \frac{2 \cdot \varphi_m}{2 \cdot \pi}} \tag{15}$$

The spindle housing was made from cast iron HT250 with surface roughness of approximately 3 μm. The material of copper tube is CuZn5 surface roughness of approximately 1.5 μm. Then the surface morphologies of the two materials were examined with a confocal laser microscope at 10X magnification.

The contact thermal resistance per unit area is defined as:

$$R_{c1} = p_{ca} \cdot \frac{k_1 + k_2}{2k_1k_2} \cdot (p_{anr1})\sigma_1 \tag{16}$$

$$R_{c2} = \frac{k_1 + k_2}{2k_1k_2} \cdot (p_{anr2})\sigma_2 \tag{17}$$

The total thermal resistance of the interface is:

$$R_{tot} = R_{bulk} + R_{c1} + R_{c2} \tag{18}$$

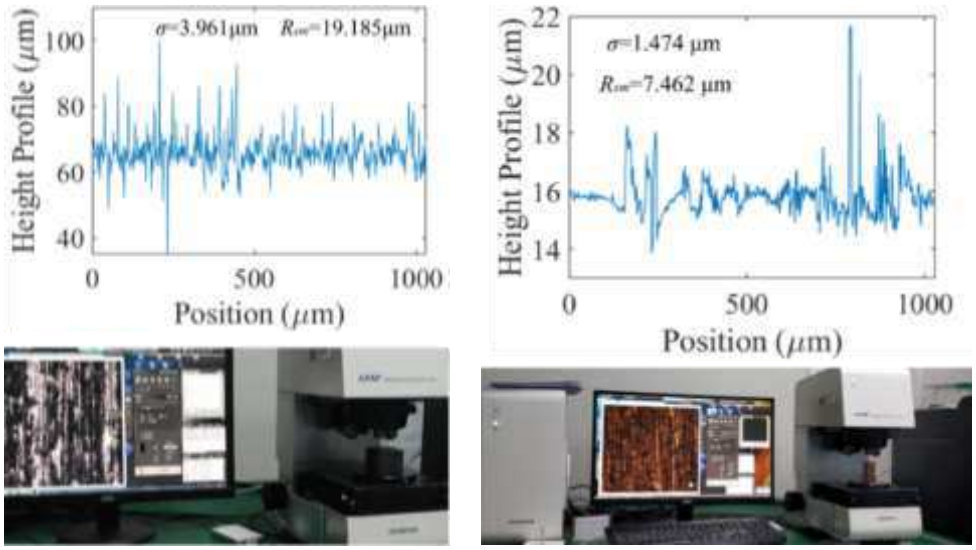

Figure 10. (a) Surface roughness measurement of cast iron (spindle housing) and (b) CuZn5 (copper tube).

The calculated bulk thermal resistance is $R_{bulk} = 2.4008 \times 10^{-4}\ \frac{m^{2} \cdot ^{\circ}C}{W}$. Regarding the contact are between cast iron and silicone grease, the contact thermal resistance is $R_{c1} = 7.9692 \times 10^{-5}\ \frac{m^{2} \cdot ^{\circ}C}{W}$. For the contact between copper tube and silicone grease, the root mean square roughness σ and average peak interval R_{sm} are

relatively small, with $\sigma \approx 1.474$ μm, $R_{sm} \approx 7.462$ μm, and $R_{c1} \approx 2.2655 \times 10^{-5}$ $\frac{m^2 \cdot ℃}{W}$. Finally, the total thermal resistance is R_{tot}=3.42427× 10^{-4} $\frac{m^2 \cdot ℃}{W}$.

3.2 Simulation process and results

Readers are referred to previous work by our research group [17, 18] and literature [24-28] for boundary conditions and methods for calculating bearing heat generation, solid-solid contact thermal resistance, convective heat transfer, and transient thermal characteristics. When the coolant flows inside the helical tube, the actual Reynolds number is close to the critical Reynolds number, so a small amount of turbulence will occur, but the flow is still primarily laminar. Therefore, the helical tube will have an enhanced heat transfer effect on the coolant [29]. The contact thermal conductivity model is shown in Section 3.1.

The boundary conditions were calculated using MATLAB and the results are shown in Table 2.

Table 2 Boundary conditions

Boundary conditions	Parts	Working conditions	Calculated value
Contact thermal conductivity of joint	Inner ring of bearing and shaft		6238 $W/(m^2 \cdot ℃)$
	Outer ring of bearing and spindle sleeve		5625 $W/(m^2 \cdot ℃)$
Convection heat transfer coefficient	Between outer surface and air		9.5 $W/(m^2 \cdot ℃)$
Bearing heat generation rate	Angular contact ball bearings 7011C	3000 rpm	66100 W/m^3
	Angular contact ball bearings 7013C	3000 rpm	90900 W/m^3
	Angular contact ball bearings 7011C	1500 rpm	28456 W/m^3
	Angular contact ball bearings 7013C	1500 rpm	39131 W/m^3
Ambient temperature		Constant temperature	19 ℃
Coolant flow state	Helical tube	*Re* = 7234	Laminar

Before conducting the finite element simulation, extraneous structures in the

spindle model, such as bolts, holes, grooves, fillets, chamfers, and so on were removed because they have little influence on heat transfer in the spindle.

The complex gear transmission mechanism, motors, and bearings in the spindle were also simplified. The material properties of the main components in the spindle are shown in Table 3.

Table 3 Spindle material properties

Material properties	Elasticity modulus E (N/m^2)	Poisson's ratio μ	Mass density ρ (kg/m^3)	2/5000 Specific heat c ($J/kg \cdot °C$)	Thermal conductivity k ($W/m \cdot °C$)	Thermal expansion coefficient α ($1 \times 10^{-6}/°C$)
Gr15(bearings)	2.19×10^{11}	0.300	7830	460	44	12
HT250 (spindle housing)	1.38×10^{11}	0.156	7280	510	45	8.2
Copper alloy (helical tube)	1.10×10^{11}	0.340	8300	381	401	18
45Cr shaft	2.11×10^{11}	0.277	7870	460	44	12
45# spindle housing	2.09×10^{11}	0.269	7280	450	48	11.7

Transient heat-fluid-structure coupling simulation results include the temperature distribution of the coolant in the helical tube, the temperature field, and the deformation field of the spindle at each point in time. Figure 11 shows simulation results when the coolant temperature is initially 18 ℃.

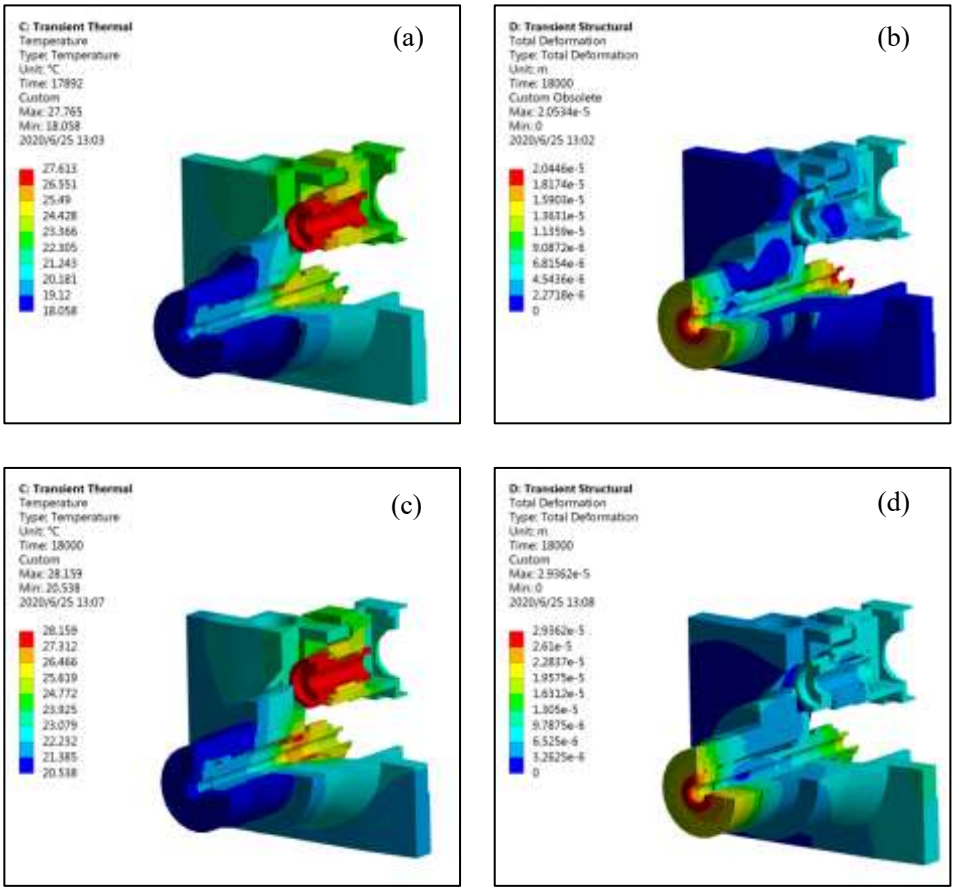

Figure 11. Thermal simulation results: (a) 16 ℃ temperature field; (b) 16 ℃ thermal deformation field; (c) 18 ℃ temperature field; (d) 18 ℃ thermal deformation field.

4 The development and experimental verification of the cooling system

4.1 External cooling system

The contact thermal resistance is very large when the rough metal surfaces are in direct contact. As shown in Figure 12. (a), applying thermal grease with sufficient thickness can increase the heat transfer efficiency between the helical tube cooler and the binding surface of the spindle housing. Convective heat transfer between the copper tube and outside air may cause instability and uncontrollable cooling. When the coolant temperature is lower than room temperature, the copper tube will reduce cooling efficiency due to convective heat transfer between the copper tube and air. The thermal insulation layer was wrapped around the helical tube to prevent convective heat transfer in air.

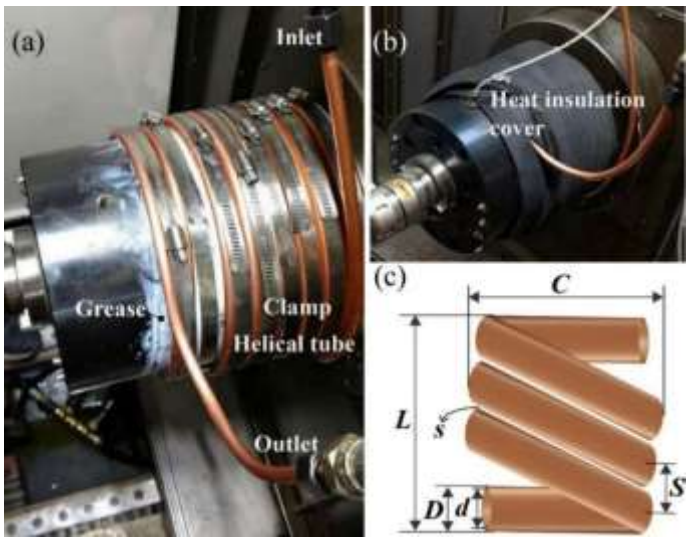

Figure 12. A boring machine spindle with helical tube: (a) installation of the cooler; (b) cooler with insulation; (c) geometry of the helical tube.

A block diagram of the spindle cooling control system is shown in Figure 13. A PLC controller (Siemens S7-200) was used to implement a control algorithm, and an industrial control computer (Advantech) was used to run Force Control configuration software to monitor the state of the system. No. 4 spindle oil was used as the cooling medium as it is used in other temperature control systems for the boring machine shown in Figure 12. Coolant circulation starts from the coolant temperature controller, is pressurized by a circulating pump, coolant flows through a turbine flowmeter and control valve, and coolant is output to the helical tube cooler. Coolant then circulates back to the temperature controller. A temperature sensor (PT100) and pressure sensor were installed at the inlet and outlet of helical tube. A temperature sensor was also installed in the position where the spindle is cooled to monitor the system temperature.

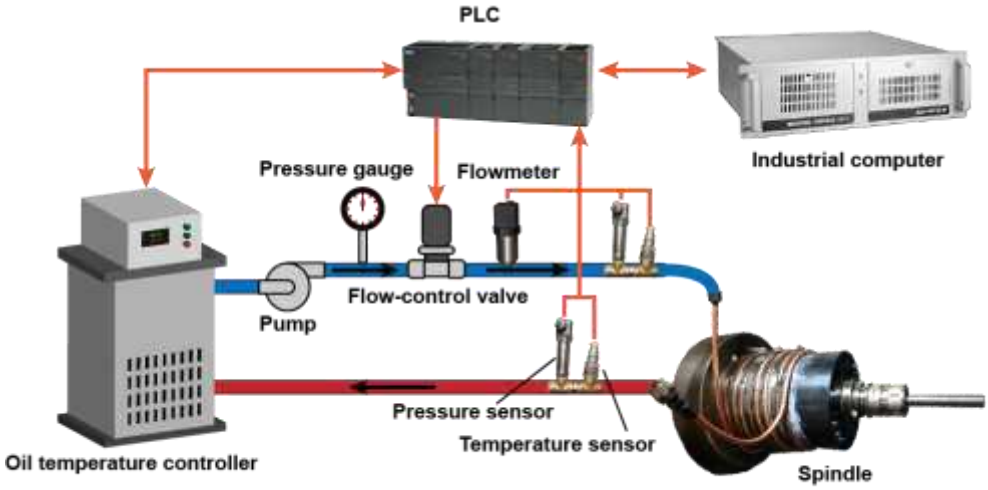

Figure 13. Design of the temperature control system.

4.2 Comparison between experimental and simulations results

The spindle experiment in this paper was conducted at constant speed. The ambient temperature of the experiment was held constant at 19 °C. The coolant was set to 20, 18, and 16 °C in experiments, and a control experiment was run without coolant. The spindle maintained a constant speed during the experiment and ran until the thermal elongation of the spindle stabilized, i.e., once the system reached thermal equilibrium. The fluid-heat-solid coupling simulation method was used in Ansys Workbench.

Figure 14 shows simulation results and experimental results when the spindle speed was set to 1500 rpm. The uncooled spindle exhibited thermal error (spindle thermal elongation) that stabilizes after approximately 250 min with maximum thermal error exceeding 30 μm.

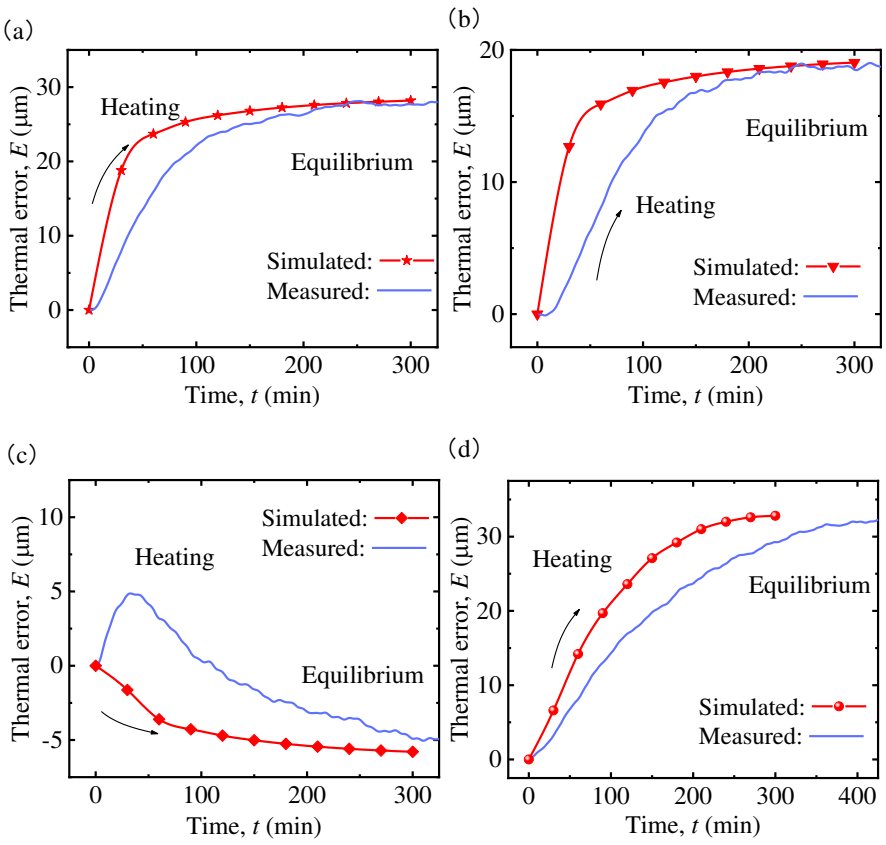

Figure 14. Experimental and simulated thermal error in the spindle rotating at 1500 rpm with coolant temperature (a) TC = 20 °C, (b) TC = 18 °C, and (c) TC = 16 °C. (d) Results for an uncooled spindle.

Figure 14. (a-c) show comparisons of experimental and simulation results for spindles cooled with 20, 18, and 16 °C coolant, respectively. The spindle system stabilizes after approximately 100 min (20 and 18 °C coolant) or 150 min (16 °C coolant). For the 20, 18, and 16 °C coolant, the maximum thermal error is

approximately 27.5, 18, and -5 μm.The results show that the simulation model roughly simulates the transient trend in thermal error, while the calculation of thermal error in equilibrium is very accurate. This substantiates the validity of the heat generation model and thermal resistance model proposed in this paper.

Regarding the results in Figure 14. (c), the thermal error tends to stabilize after approximately 150 minutes. In this group of experiments, due to the complexity of the spindle in the initial stage of operation and unavoidable errors in the calculated boundary conditions, the simulated and experimental thermal error values exhibit different trends at the beginning of the experiment. However, as time progresses, the simulation results become more accurate as thermal equilibrium is reached. The uncooled spindle reaches thermal equilibrium at approximately 300 min, which is much longer than the time required to reach thermal equilibrium when a cooler is used.

Due to the complexity of the initial state of the machine tool and errors in the calculated boundary conditions, the transient simulation results do not perfectly match the experimental measurements. The root mean square error (RMSE) between the simulated and experimental thermal error values was used to quantify accuracy. The RMSE value found in the experiment is shown in Table 4.

Table 4 RMSE for thermal error when the spindle speed is 1500 rpm

Coolant temperature (℃)	Uncooled	20 ℃	18 ℃	16 ℃
RMSE (μm)	5.7044	4.3592	4.1636	3.8535

The values in Table 4 show that, when the spindle speed is 1500 rpm, the uncooled spindle has the largest RMSE value of 5.7044 μm. The spindle with 16 ℃ coolant has the smallest RMSE value of 3.8535 μm. All of the RMSE values are found to be within a reasonable range, and the error between the simulated and experimental results is small, indicating that the calculation of the boundary conditions in this simulation is more accurate.

Figure 15 shows a comparison between simulated and experimental results when the spindle speed is 3000 rpm.

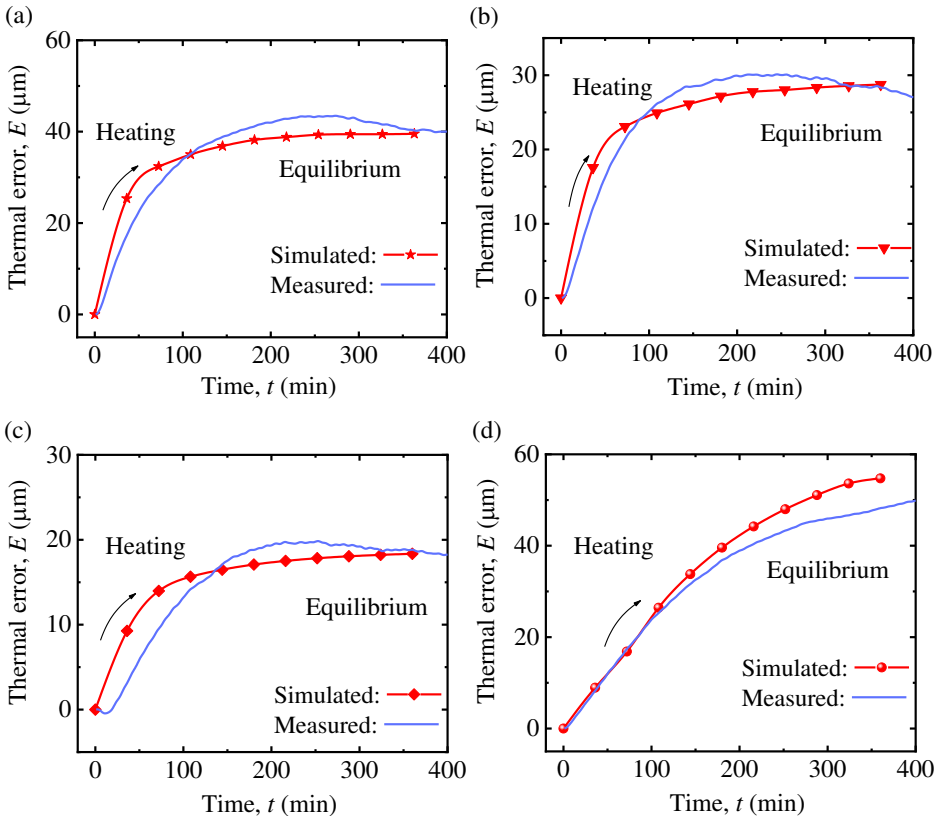

Figure 15. Comparison between simulated and experimental thermal error for a spindle rotating at 3000 rpm with coolant temperature (a) TC = 20 ℃, (b) TC = 18 ℃, and (c) TC = 16 ℃. (d) Results for an uncooled spindle.

The thermal error of the uncooled spindle system tends to stabilize after 300 min, and the maximum thermal error is greater than 50 μm. For this rotation speed, the simulation curve is more consistent with the experimental results. Figure 15. (a-c) shows the thermal error when the coolant temperature was held constant at 20, 18, and 16 ℃, respectively. The thermal error of the spindle system tends to stabilize after approximately 100 min. Figure 15 (d) shows the same comparison for an uncooled spindle; this system takes longer than 300 min to reach thermal equilibrium. Comparing the experimental results for the cooled and uncooled spindles, one can see that the external cooler can be used to effectively reduce the thermal error during operation, so that the spindle system reaches thermal equilibrium earlier. Thus, the cooling control method can effectively cause the temperature distribution of the spindle system to become uniform and quickly stabilize over a shorter time period.

The RMSE between the simulated and experimental thermal error for the spindle rotating at 3000 rpm is shown in Table 5.

Table 5 RMSE for thermal error when the spindle speed is 3000 rpm

Coolant temperature (℃)	Uncooled	20 ℃	18 ℃	16 ℃
RMSE (μm)	3.9714	3.6507	2.2582	2.5982

When the rotation speed of the spindle is 3000 rpm, the uncooled spindle exhibits the largest RMSE value of 3.9714 μm. The spindle with 18 ℃ coolant has the smallest RMSE of 2.2582 μm. The RMSE values are all within a reasonable range, indicating that the simulation results are consistent with the experimental results.

5 Conclusions

A model describing contact thermal resistance between silicone grease and a solid metal substrate and a model describing the total thermal resistance for a solid-solid interface filled with silicone grease are presented in this paper. Experimental and simulated results show that these models reflect the variation in thermal resistance with the pressure between the interfaces and thickness of the silicone grease. The model was used to calculate the total thermal resistance for the cambered-flat interface between the cooler and the spindle. The model was used for transient thermal-fluid-solid coupling simulations.

Because the pressure between the interfaces is small, the thermal conductivity of the selected silicone grease is high, thus the surface roughness of the cast iron is relatively large, and the contact thermal resistance between the metal and silicone grease accounts for 29.8% of the total thermal resistance.

The external cooling system decreases the time required to reach thermal equilibrium time by more than 60%, and the absolute value of the thermal error is significantly reduced.

The simulation can be used to predict the thermal equilibrium time and accurately reflect the influence of the coolant temperature T_C. The predicted RMSE value in the axial thermal error for the 3000 rpm spindle condition is less than 5.7044 μm, and the predicted RMSE value in the axial thermal error for the 1500 rpm spindle is less than 3.9714 μm.

Acknowledgments

The author(s) disclosed receipt of the following financial support for the research, authorship, and/or publication of this article: Shaanxi Science and Technology Major Project (2019zdzx01-02-02), Key R&D Program of Shaanxi (2020ZDLGY14-04), National Natural Science Foundation of China (No. 51975465), China Postdoctoral

Science Foundation (2019M660251).

Author contribution Liang Zhao designed the study, performed experiments, and wrote the manuscript; Mohan Lei, Hongdi Ren and Shuai Wang designed the study and contributed to the data interpretation.

Availability of data and material Data and materials are available.

Code availability Not applicable.

Declarations

Ethics approval Not applicable.

Consent to participate I am agreeing to participate.

Consent for publication I am agreeing to publish this work.

Conflict of interest The authors declare no competing interests.

References

1.Mayr, J., et al., Thermal issues in machine tools. CIRP Annals, 2012. 61(2): p. 771-791.

2. Shi, H., et al., Investigation into effect of thermal expansion on thermally induced error of ball screw feed drive system of precision machine tools. International Journal of Machine Tools and Manufacture, 2015. 97: p. 60-71.

3. Li, Y., et al., A review on spindle thermal error compensation in machine tools. International Journal of Machine Tools and Manufacture, 2015. 95: p. 20-38.

4. Ge, Z. and X. Ding, Design of thermal error control system for high-speed motorized spindle based on thermal contraction of CFRP. International Journal of Machine Tools and Manufacture, 2018. 125: p. 99-111.

5. Donmez, M.A., M.H. Hahn, and J.A. Soons, A Novel Cooling System to Reduce Thermally-Induced Errors of Machine Tools. CIRP Annals, 2007. 56(1): p. 521-524.

6.Dornfeld, D. and D.E.J.S.B. Lee, Precision Manufacturing. 2008.

7. Xia, C., et al., Conjugate heat transfer in fractal tree-like channels network heat sink for high-speed motorized spindle cooling. Applied Thermal Engineering, 2015. 90: p. 1032-1042.

8. Liu, T., et al., A differentiated multi-loops bath recirculation system for precision machine tools. Applied Thermal Engineering, 2015. 76: p. 54-63.

9. Bossmanns, B. and J.F. Tu, A power flow model for high speed motorized spindles - Heat generation characterization. Journal of Manufacturing Science and Engineering-Transactions of the Asme, 2001. 123(3): p. 494-505.

10. Madhusudana, C.V., Thermal contact conductance / C.V. Madhusudana. Mechanical engineering series (Berlin, Germany). 1996, New York: Springer-Verlag.

11. Bajracharya, I., et al., Characterization of Thermal Contact Resistance Doped with Thermal Interface Material. Journal of the Korean Society for Precision Engineering, 2013. 30(9): p. 943-950.

12. Prasher, R.S., Surface Chemistry and Characteristics Based Model for the Thermal Contact Resistance of Fluidic Interstitial Thermal Interface Materials. Journal of Heat Transfer, 2001. 123(5): p. 969-975.

13. Yuan, C., et al., An improved model for predicting thermal contact resistance at liquid–solid interface. International Journal of Heat and Mass Transfer, 2015. 80: p. 398-406.

14. Hamasaiid, A., et al., A predictive model for the thermal contact resistance at liquid–solid interfaces: Analytical developments and validation. International Journal of Thermal Sciences, 2011. 50(8): p. 1445-1459.

15. Hamasaiid, A., et al., A predictive model for the evolution of the thermal conductance at the casting–die interfaces in high pressure die casting. International Journal of Thermal Sciences, 2010. 49(2): p. 365-372.

16. Jianbin, Z. and L. Hongwei. Thermal performance analysis for the machine tool's spindle. in 2012 7th IEEE Conference on Industrial Electronics and Applications (ICIEA). 2012.

17. Ma, C., et al., Simulation and experimental study on the thermally induced deformations of high-speed spindle system. Applied Thermal Engineering, 2015. 86: p. 251-268.

18. Yang, J., et al., Experiments and simulation of thermal behaviors of the dual-drive servo feed system. Chinese Journal of Mechanical Engineering, 2015. 28(1): p. 76-87.

19. Prasher, R.S., et al. Thermal resistance of particle laden polymeric thermal interface materials. in ASME 2003 International Mechanical Engineering Congress and Exposition. 2003. American Society of Mechanical Engineers.

20. Yuan, C., Z. Peng, and X. Yan, Surface Characterization Using Wavelet Theory

and Confocal Laser Scanning Microscopy. Journal of Tribology, 2005. 127(2): p. 394-404.

21. Chao, Y., Thermal resistance model and conductivity enhancement of thermal interface materials. 2017, Huazhong University of science and technology

22. Committee, A.D., Standard Test Method for Thermal Transmission Properties of Thermally Conductive Electrical Insulation Materials. ASTM International, West Conshohocken, PA, Standard No. ASTM D5470-06. https://www. astm. org/DATABASE. CART/HISTORICAL/D5470-06. htm, 2012.

23. Prasher, R.S., et al., Rheological Study of Micro Particle Laden Polymeric Thermal Interface Materials: Part 2 — Modeling. 2002(3638X): p. 53-59.

24.Harris, T.A., Rolling bearing analysis. 2001: John Wiley and sons.

25. Dravid, A.N., et al., Effect of secondary fluid motion on laminar flow heat transfer in helically coiled tubes. AIChE Journal, 1971. 17(5): p. 1114-1122.

26. Patankar, S.V. and D.B. Spalding, A calculation procedure for heat, mass and momentum transfer in three-dimensional parabolic flows. International Journal of Heat and Mass Transfer, 1972. 15(10): p. 1787-1806.

27. Su, H., et al., Thermal analysis of the hydrostatic spindle system by the finite volume element method. The International Journal of Advanced Manufacturing Technology, 2014. 71(9): p. 1949-1959.

28. Schmucker, H., F. Flemming, and S. Coulson, Two-way coupled fluid structure interaction simulation of a propeller turbine. IOP Conference Series: Earth and Environmental Science, 2010. 12(1): p. 012011.

29. Al, F.P.I.E., Fundamentals of Heat and Mass Transfer 6th Ed. 2007: Wiley. 139–162.

Figures

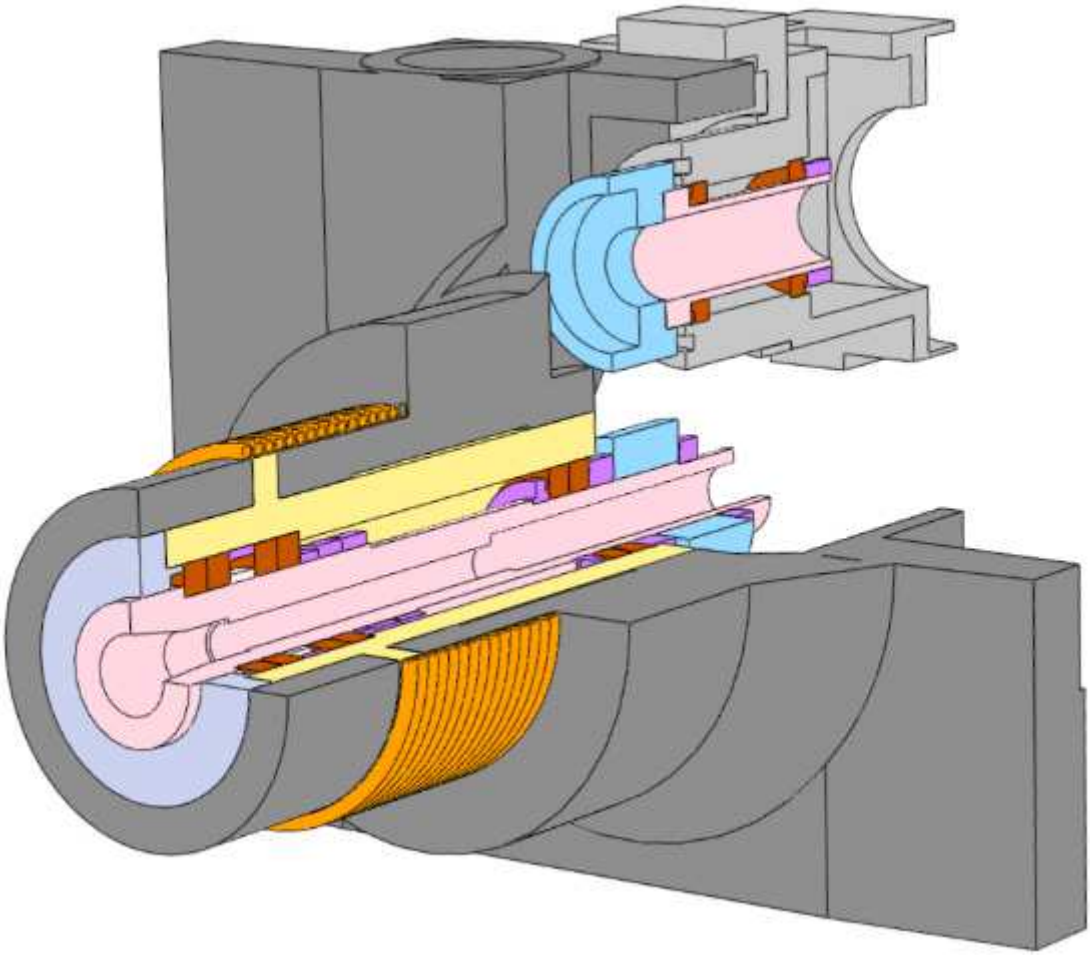

Figure 1

Helically coiled tube cooler.

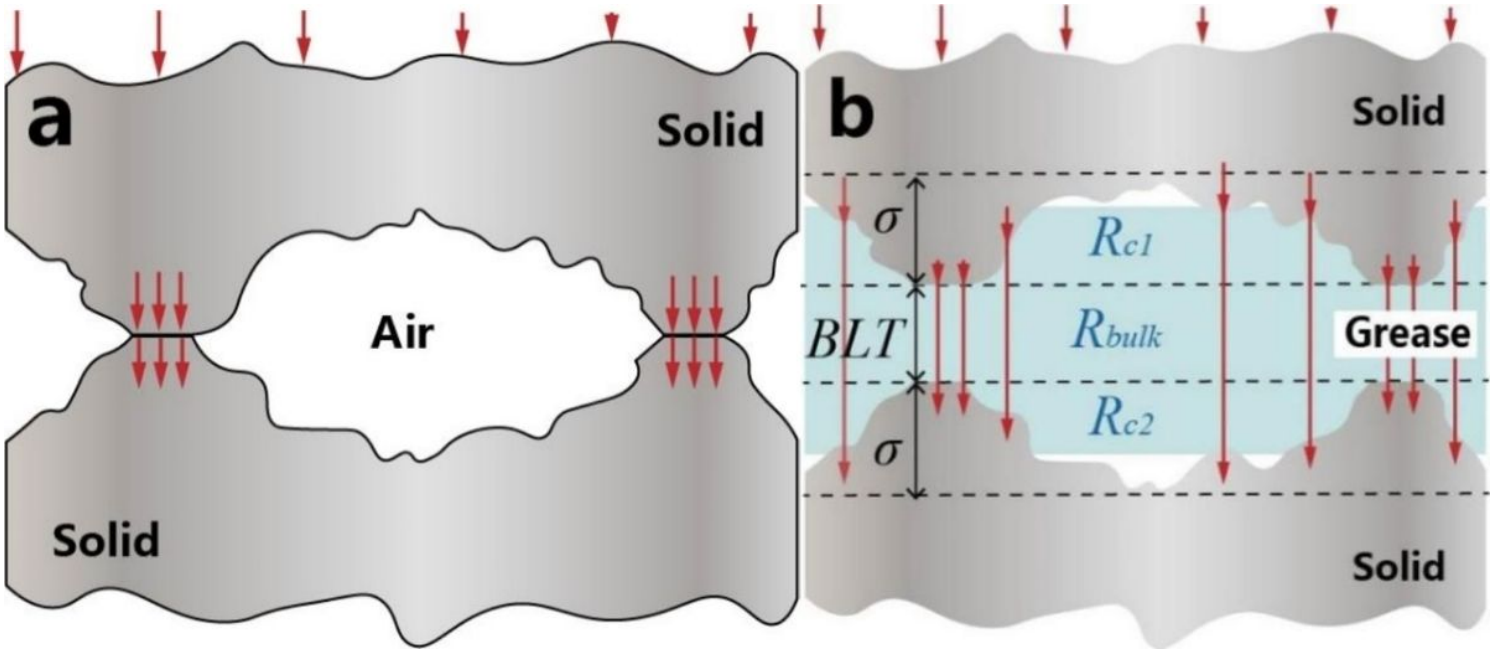

Figure 2

Heat conduction of joint surface; (a) rough metal joint surface and (b) metal interface filled with silicone grease.

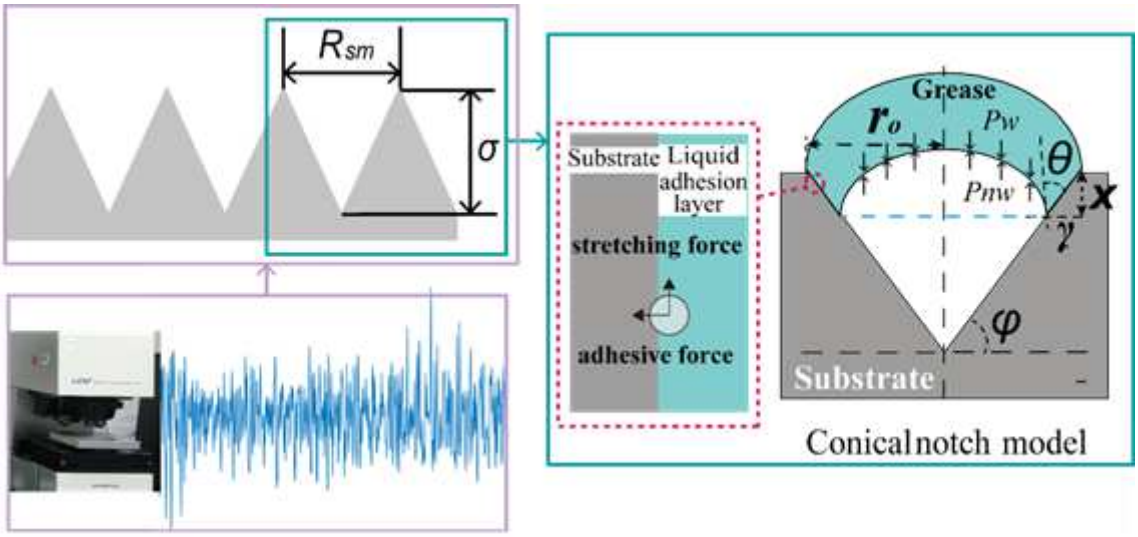

Figure 3

Conical groove model based on surface roughness.

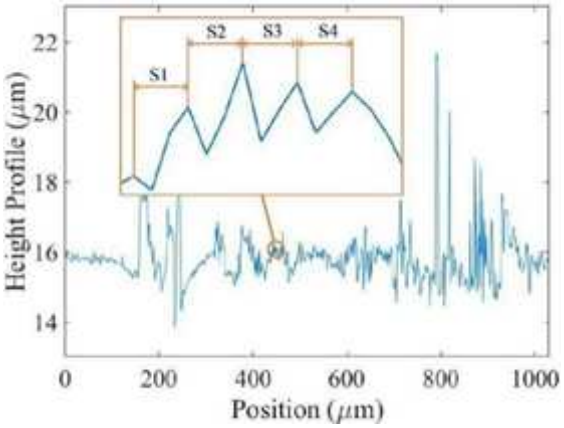

Figure 4

Average peak spacing in rough surface profile.

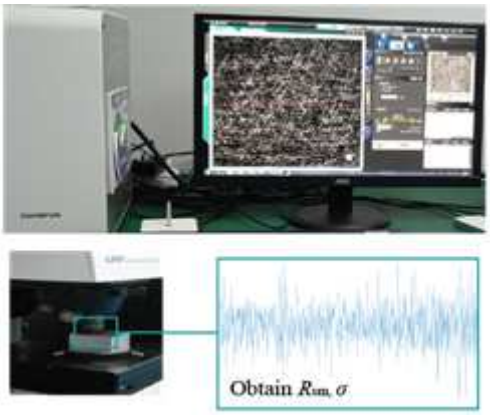

Figure 5

Rough topography measurement.

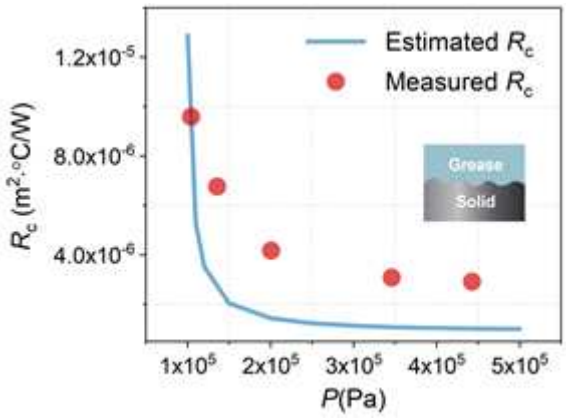

Figure 6

Comparison between calculated and experimental contact thermal resistance between aluminum and silicone grease.

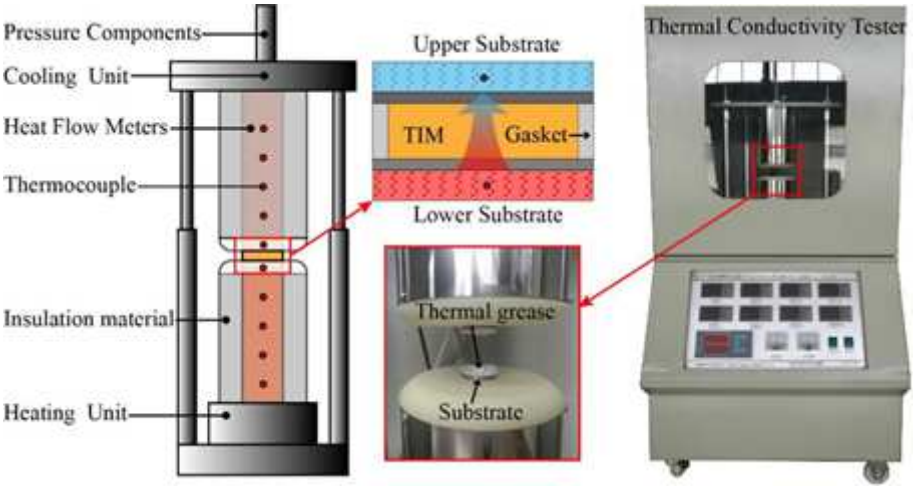

Figure 7

Silicone grease thermal conductivity tester

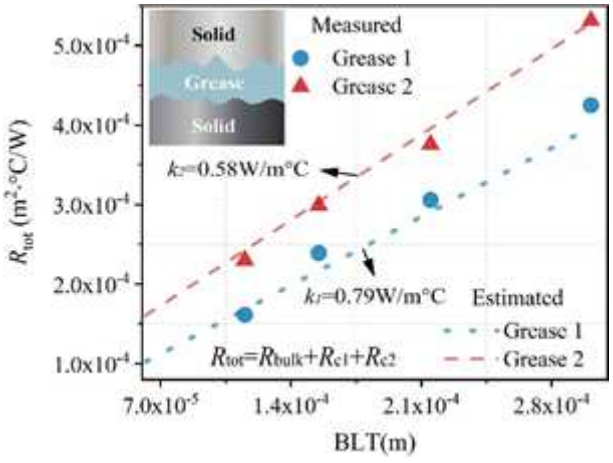

Figure 8

Comparison between calculated and experimental total thermal resistance between copper substrates filled with silicone grease.

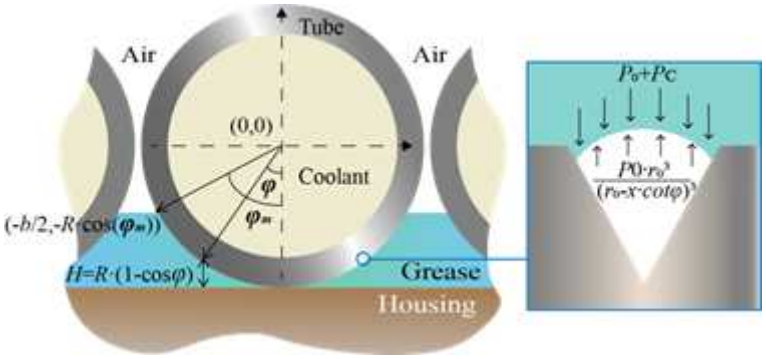

Figure 9

Copper tube-silicone grease-spindle shell contact cross section.

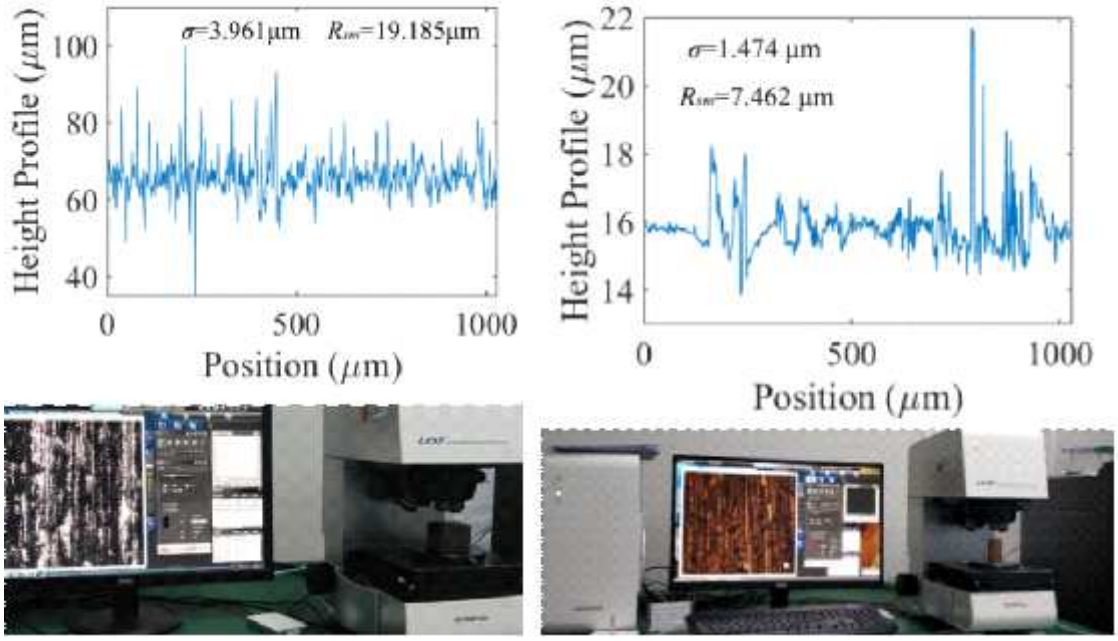

Figure 10

(a) Surface roughness measurement of cast iron (spindle housing) and (b) CuZn5 (copper tube).

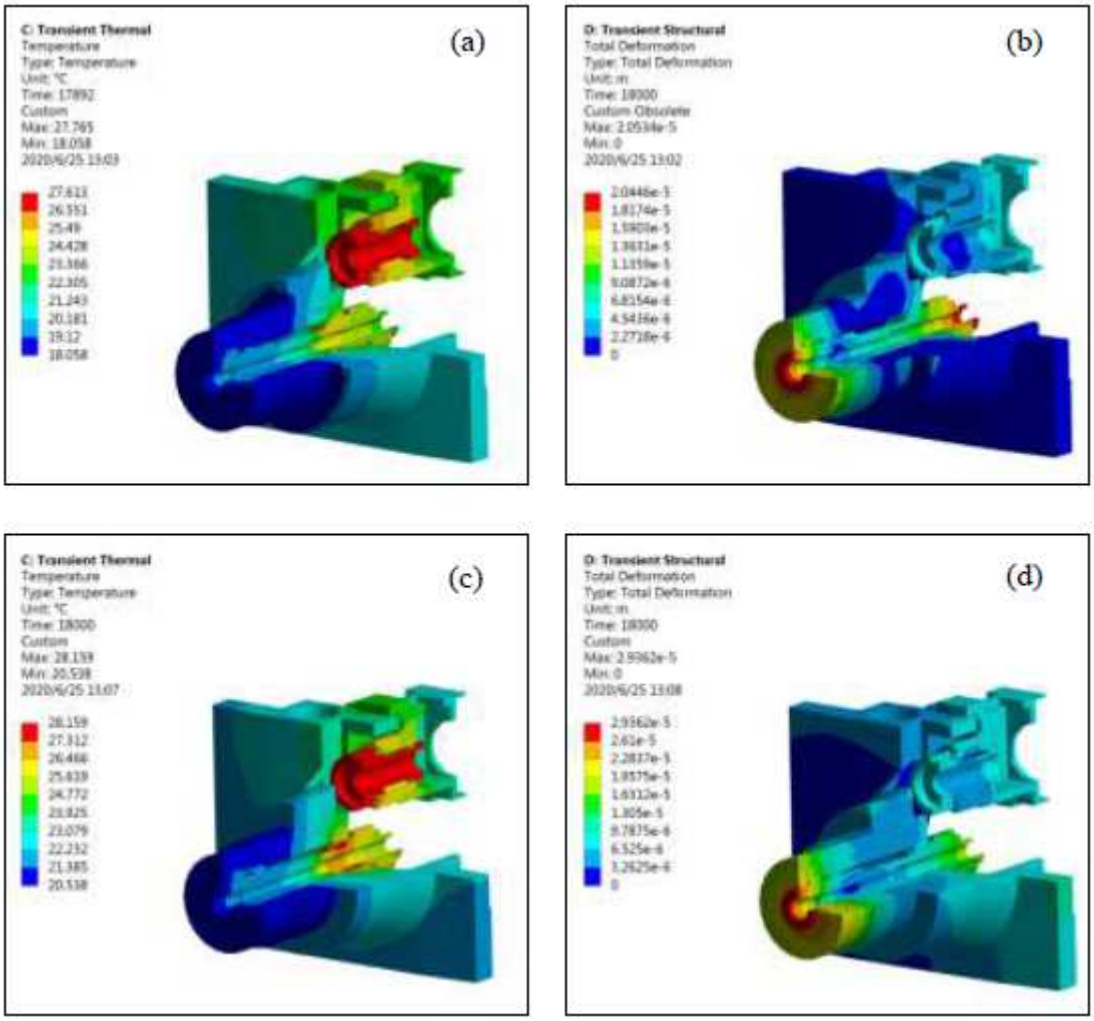

Figure 11

Thermal simulation results: (a) 16 ℃ temperature field; (b) 16 ℃ thermal deformation field; (c) 18 ℃ temperature field; (d) 18 ℃ thermal deformation field.

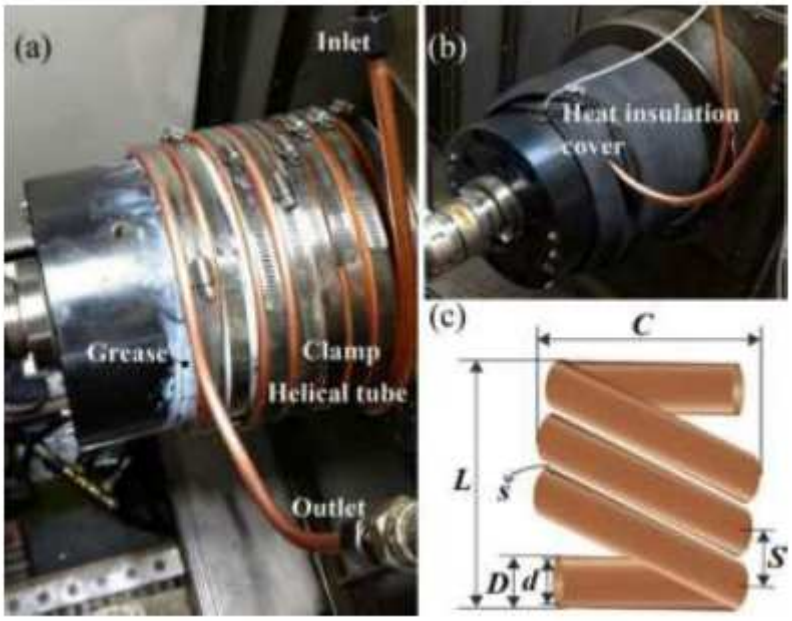

Figure 12

A boring machine spindle with helical tube: (a) installation of the cooler; (b) cooler with insulation; (c) geometry of the helical tube.

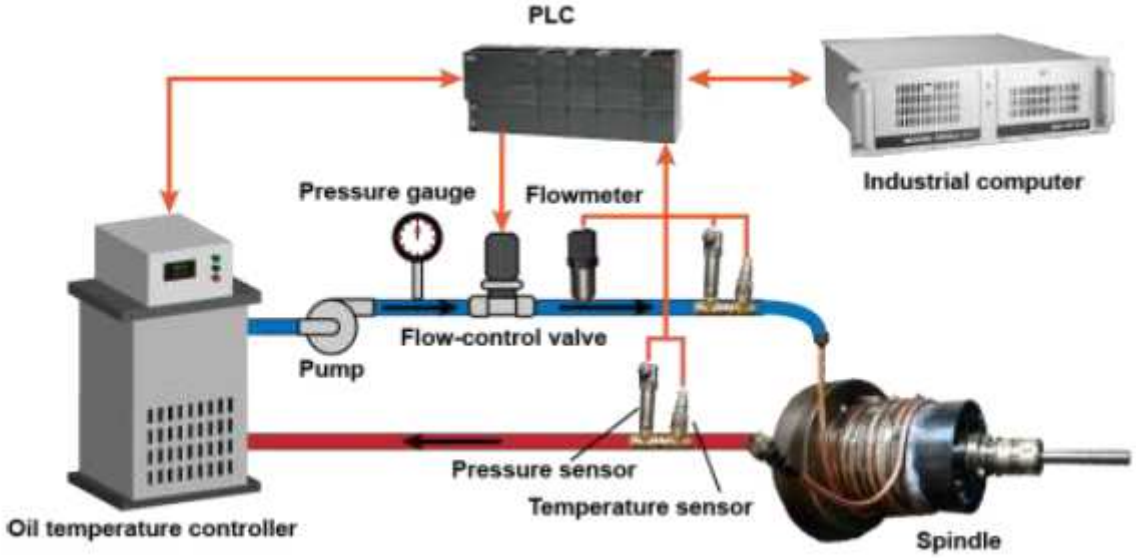

Figure 13

Design of the temperature control system.

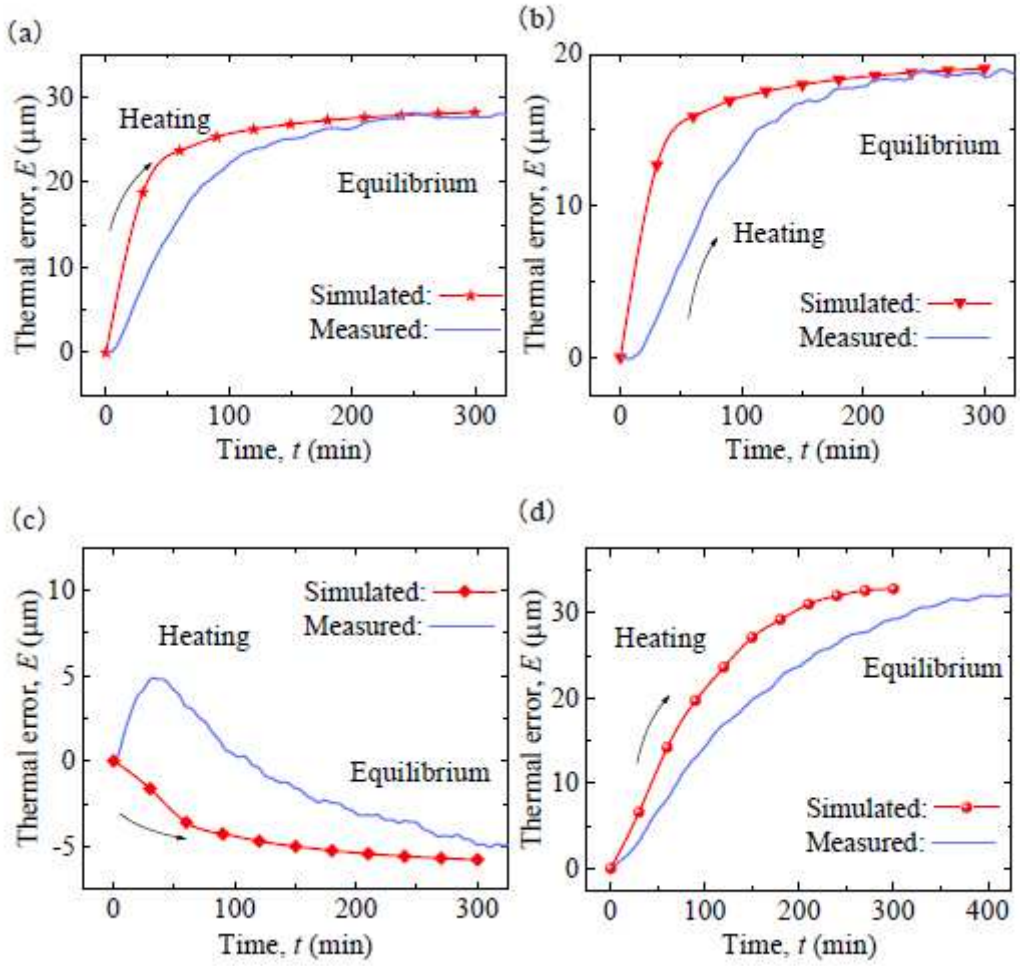

Figure 14

Experimental and simulated thermal error in the spindle rotating at 1500 rpm with coolant temperature (a) TC = 20 ℃, (b) TC = 18 ℃, and (c) TC = 16 ℃. (d) Results for an uncooled spindle.

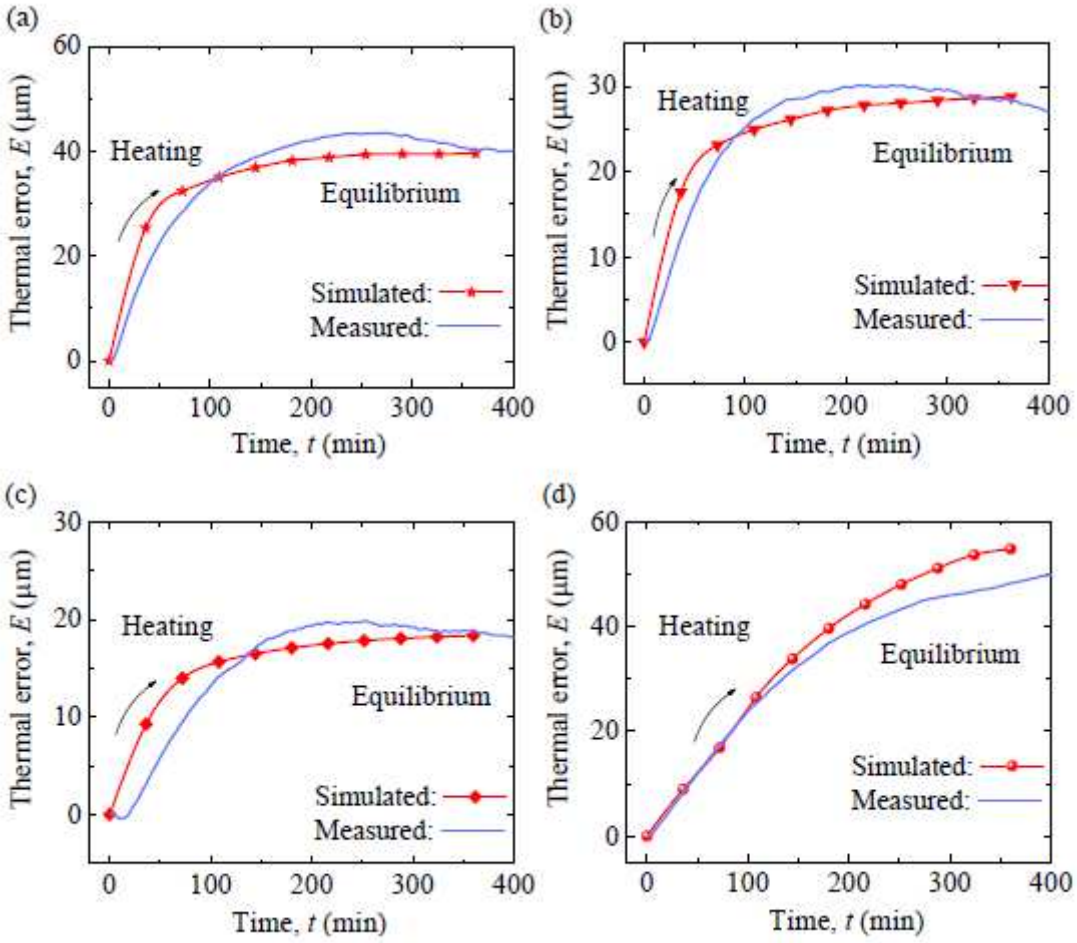

Figure 15

Comparison between simulated and experimental thermal error for a spindle rotating at 3000 rpm with coolant temperature (a) TC = 20 ℃, (b) TC = 18 ℃, and (c) TC = 16 ℃. (d) Results for an uncooled spindle.